Investigating the Impact of Reemerging Sea Surface Temperature Anomalies on the Winter Atmospheric Circulation over the North Atlantic

CHRISTOPHE CASSOU

CNRS–CERFACS, Toulouse, France, and National Center for Atmospheric Research, Boulder, Colorado

CLARA DESER

National Center for Atmospheric Research, Boulder, Colorado

MICHAEL A. ALEXANDER

NOAA/Earth System Research Laboratory, and Climate Diagnostics Center, Boulder, Colorado

(Manuscript submitted 30 March 2006, in final form 15 November 2006)

ABSTRACT

Extratropical SSTs can be influenced by the "reemergence mechanism," whereby thermal anomalies in the deep winter mixed layer persist at depth through summer and are then reentrained into the mixed layer in the following winter. The impact of reemergence in the North Atlantic Ocean (NAO) upon the climate system is investigated using an atmospheric general circulation model coupled to a mixed layer ocean/thermodynamic sea ice model.

The dominant pattern of thermal anomalies below the mixed layer in summer in a 150-yr control integration is associated with the North Atlantic SST tripole forced by the NAO in the previous winter as indicated by singular value decomposition (SVD). To isolate the reemerging signal, two additional 60-member ensemble experiments were conducted in which temperature anomalies below 40 m obtained from the SVD analysis are added to or subtracted from the control integration. The reemerging signal, given by the mean difference between the two 60-member ensembles, causes the SST anomaly tripole to recur, beginning in fall, amplifying through January, and persisting through the following spring. The atmospheric response to these SST anomalies resembles the circulation that created them the previous winter but with reduced amplitude (10–20 m at 500 mb per °C), modestly enhancing the winter-to-winter persistence of the NAO. Changes in the transient eddies and their interactions with the mean flow contribute to the large-scale equivalent barotropic response throughout the troposphere. The latter can also be attributed to the change in occurrence of intrinsic weather regimes.

1. Introduction

It is well established that the nonseasonal variability of the atmospheric circulation over the North Atlantic sector is primarily governed by internal dynamical processes resulting in chaotic temporal behavior and a reduction in potential predictability on time scales longer than a week or two (Rodwell 2003). This "climate noise" paradigm (Madden 1976) has been shown to be highly relevant for the North Atlantic Oscillation (NAO), the leading mode of atmospheric variability over the North Atlantic (Wunsch 1999; Stephenson et al. 2000; Feldstein 2000). However, the temporal behavior of the NAO appears to be modulated slightly by external forcing and/or coupling to other components of the climate system, particularly the oceans (see Hurrell et al. 2003 for a review). This departure from random behavior is evident, for example, in the enhanced variance and persistence of the NAO beyond that expected from climate noise alone (Feldstein 2000; Greatbatch 2000). Given the large environmental and socioeconomic impacts of the NAO over Europe and eastern North America (Hurrell 1995), it is of interest to investigate mechanisms that contribute to the nonrandom component of NAO variability. In the present study, we

Corresponding author address: Christophe Cassou, CERFACS–CNRS, 42, Avenue G. Coriolis, 31057 Toulouse, CEDEX 01, France.
E-mail: cassou@cerfacs.fr

DOI: 10.1175/JCLI4202.1

focus on understanding the role of the "oceanic reemergence mechanism" (Alexander and Deser 1995) in enhancing the year-to-year persistence of the NAO, especially during winter.

The interaction between the reemergence mechanism and the NAO can be viewed as follows. During winter, anomalous surface winds and air temperatures associated with the positive or negative phase of the NAO result in anomalous fluxes of sensible and latent heat at the sea surface, which create ocean temperature anomalies that extend down to the base of the deep winter mixed layer (Cayan 1992; Deser and Timlin 1997; Seager et al. 2000). These thermal anomalies project onto the so-called North Atlantic tripole whose typical *e*-folding time is on the order of 3–5 months at the surface (see a review in Frankignoul 1985). At depth, the anomalies persist through spring and summer within the stably stratified seasonal thermocline, insulated from thermal damping to the atmosphere by the formation of a shallow mixed layer in response to increasing solar radiation and weakening stirring due to slackened surface winds. Their sequestration ends in the following fall or early winter when the mixed layer deepens again due to the seasonal intensification of the extratropical atmospheric circulation, and the thermal anomalies created the previous winter become reentrained into the mixed layer, affecting sea surface temperatures (SSTs). This reentrainment thus leads to the "*reemergence*" of the previous winter's SST anomalies. Oceanic reemergence occurs basinwide both in the Pacific (Alexander et al. 1999) and the Atlantic (Timlin et al. 2002; de Coëtlogon and Frankignoul 2003), and its timing and intensity are functions of the depth of the winter mixed layer and the strength of the anomalous wintertime atmospheric forcing. The persistence of the NAO-forced SST anomaly tripole pattern from one winter to the next has been shown to be consistent with the reemergence mechanism (Watanabe and Kimoto 2000; Timlin et al. 2002; Deser et al. 2003; de Coëtlogon and Frankignoul 2003).

Here we investigate to what extent the reemergence mechanism affects the overlying atmosphere including the winter-to-winter persistence of the NAO. While addressing this question, we have to keep in mind though that the dominant source of the NAO variability is internal atmospheric dynamics. As claimed in Junge and Haine (2001) for the ocean, it is evident that even if reemergence does play a role, contemporaneous heat flux anomalies are much more effective at generating wintertime SST anomalies. For the atmosphere, Kushnir et al. (2002) state that external forcings all together could explain at most 20%–25% of the interannual variance of the North Atlantic atmosphere. Nevertheless, as pointed out in the Kushnir et al. review, much can be gained in seasonal-to-interannual prediction from better resolving and understanding all the weakly coupled processes involved in North Atlantic climate, which could have a significant impact under particular conditions.

Isolating and quantifying the role of oceanic reemergence upon the atmospheric circulation in observations and fully coupled models is difficult because of the dominance of atmospheric forcing of the underlying ocean. In this study, we perform experiments with an atmospheric general circulation model (AGCM) coupled to an entraining ocean mixed layer/thermodynamic sea ice models in which oceanic thermal anomalies are imposed beneath the shallow mixed layer in summer, and the coupled system is allowed to respond over the ensuing fall and winter. Such experiments include the reemergence mechanism as well as air–sea ice exchanges that have been shown to influence the North Atlantic atmospheric variability. The experiment design also allows for the simulation of a reasonable mean ocean climate via a flux correction term that mainly compensates for the absence of oceanic heat transport (and to a lesser extent for model biases). On the other hand, we omit any nonlocality of the reemergence mechanism due to neglected oceanic advection that may add some persistence to the wintertime SST anomalies and associated atmospheric circulation as suggested by de Coëtlogon and Frankignoul (2003).

The paper is organized as follows. The atmosphere, ocean, and ice components of the coupled model, the method of coupling, and the model performance are described in section 2. The experimental design chosen to isolate, quantify, and understand the impact of the reemergence on the North Atlantic atmosphere is presented in section 3. The simulated atmospheric response to reemerging thermal ocean anomalies is examined in section 4. Processes involved in the atmospheric response, their timing, and their amplitude, are also explored. The results are summarized and further discussed in section 5.

2. Coupled model description and performance

a. Model components

The coupled model used in this study has four components. The model atmosphere is the second version of the National Center for Atmospheric Research (NCAR) Community Atmosphere Model (CAM2.1). The dynamical core of this AGCM is based upon an Eulerian spectral scheme solved on a Gaussian grid of about $2.8° \times 2.8°$ latitude–longitude corresponding to a

triangular horizontal truncation at 42 wavenumbers. The vertical resolution is discretized over 26 levels using a progressive hybrid coordinate. Kiehl and Gent (2004) provide a detailed description of the model and evaluate its performance. The land surface and the sea ice components are the Community Land Model (CLM2; Oleson et al. 2004) and the Community Sea Ice Model (CSIM; Briegleb et al. 2004), respectively. The dynamical core of the latter has been turned off in the present case. The ocean component consists of independent single-column models with explicit mixed layer physics and no horizontal advection. Land, sea ice, and ocean models are aligned with the CAM grid. Coupling between the ocean and the other components occurs daily, while the atmosphere, ice, and land modules exchange flux and mass quantities at the CAM time step.

The ocean mixed layer model (MLM) is based on Gaspar (1988)'s formulation as implemented by Alexander and Deser (1995). In the present study, we use a modified version of that used in Alexander et al. (2000), where we include additional layers, extend the ocean bottom to 1500 m (instead of 1000 m), and implement coupling between the thermodynamical sea ice component of CSIM and the MLM surface layer. Each ocean point has 36 vertical levels with 15 layers in the upper 100 m and a realistic bathymetry. The mixed layer depth (MLD) is computed as a prognostic variable based on turbulent kinetic energy parameterization when deepening, or as a diagnostic quantity based on the balance between wind stirring and surface buoyancy forcing when shoaling. Very shallow areas ($<$40 m), however, are treated as a fixed 50-m depth slab ocean. (A complete description of the model and its equations, as well as details of the computational methods and correction terms, may be found in an electronic supplement (http://www.cgd.ucar.edu/cas/cdeser/REMsupfig.html); only a brief overview is given here.

A surface heat flux correction term (Q_{cor}) is applied to account for missing physics in the ocean such as heat transport by the mean currents and diffusion, as well as errors in the atmospheric surface fluxes to a lesser extent. The distribution of Q_{cor} in December–February and June–August (Figs. 1a,b) indicates that it adds heat to the oceans in the winter hemisphere and extract heat year-round in the deep Tropics, especially in the Pacific and Atlantic. The latter compensates for missing horizontal advection along the equatorial cold tongues and associated upwelling, while the former compensates for missing horizontal advection along the Gulf Stream and Kuroshio, in the North Atlantic and North Pacific, respectively. In June–August in the Southern Hemisphere, Q_{cor} brings heat along the storm track into the mixed layer, which is fed in nature by intrusions of warm intermediate waters and the Ekman contribution that is not simulated in MLM. A salinity flux correction term S_{cor} is also added in the model, but note that while Q_{cor} resembles the distribution of ocean heat transport in extratropical regions, S_{cor} does not reflect the distribution of the freshwater flux (Figs. 1c,d) and salt advection by the ocean is not a large contributor to S_{cor}. The term S_{cor} mainly corrects for biases in the precipitation $-$ evaporation budget and the absence of river runoff in the model. In winter (Fig. 1c), it compensates for the overestimated precipitation along the intertropical convergence zone (ITCZ) at 5°N in the Pacific, enhanced evaporation due to stronger trade winds in the subtropics, and a northward shift in the extratropical storm track. In polar regions, S_{cor} accounts for missing physics in the ice model (dynamical processes).

b. The coupled model mean state

We performed a 150-yr control integration of the coupled model, hereafter referred to as CTL. The control integration, with the inclusion of a flux correction, reproduces the observed mean SST distribution, with differences between CTL and observations generally less than $\pm$0.3°C in the Tropics year-round and in midlatitudes during winter (Figs. 1e,f). The largest errors (positive) occur in summer in the extratropical oceans due to shallower-than-observed MLD. A summertime bias of around +1°C is found basinwide in the Northern Hemisphere extratropical oceans and above the subtropical highs in the Southern Hemisphere along 40°S. Errors in sea ice extent lead to SST biases in the polar regions.

The deepest MLDs occur in the winter hemisphere in CTL (Figs. 1g,h), similar to observations (see, e.g., de Boyer Montegut et al. 2004). In the Northern Hemisphere, maxima are collocated with the storm tracks both in the North Pacific and North Atlantic with realistically simulated values between 150 and 200 m. Deeper MLDs ($\sim$250 m) are found between Greenland and Great Britain as well as in the Labrador and Norwegian Seas; however, these values are still strongly underestimated compared to observations, although a few grid points around Iceland and Spitzberg in CTL reach 600–700 m. Alexander et al. (2000) provide a discussion of the factors leading to the model's underestimate of MLD in regions of deep-water formation.

There is no significant drift in MLD, temperature, and salinity away from coastal grid points over the 150-yr duration of CTL. However a clear trend in salinity is found beneath sea ice grid points.

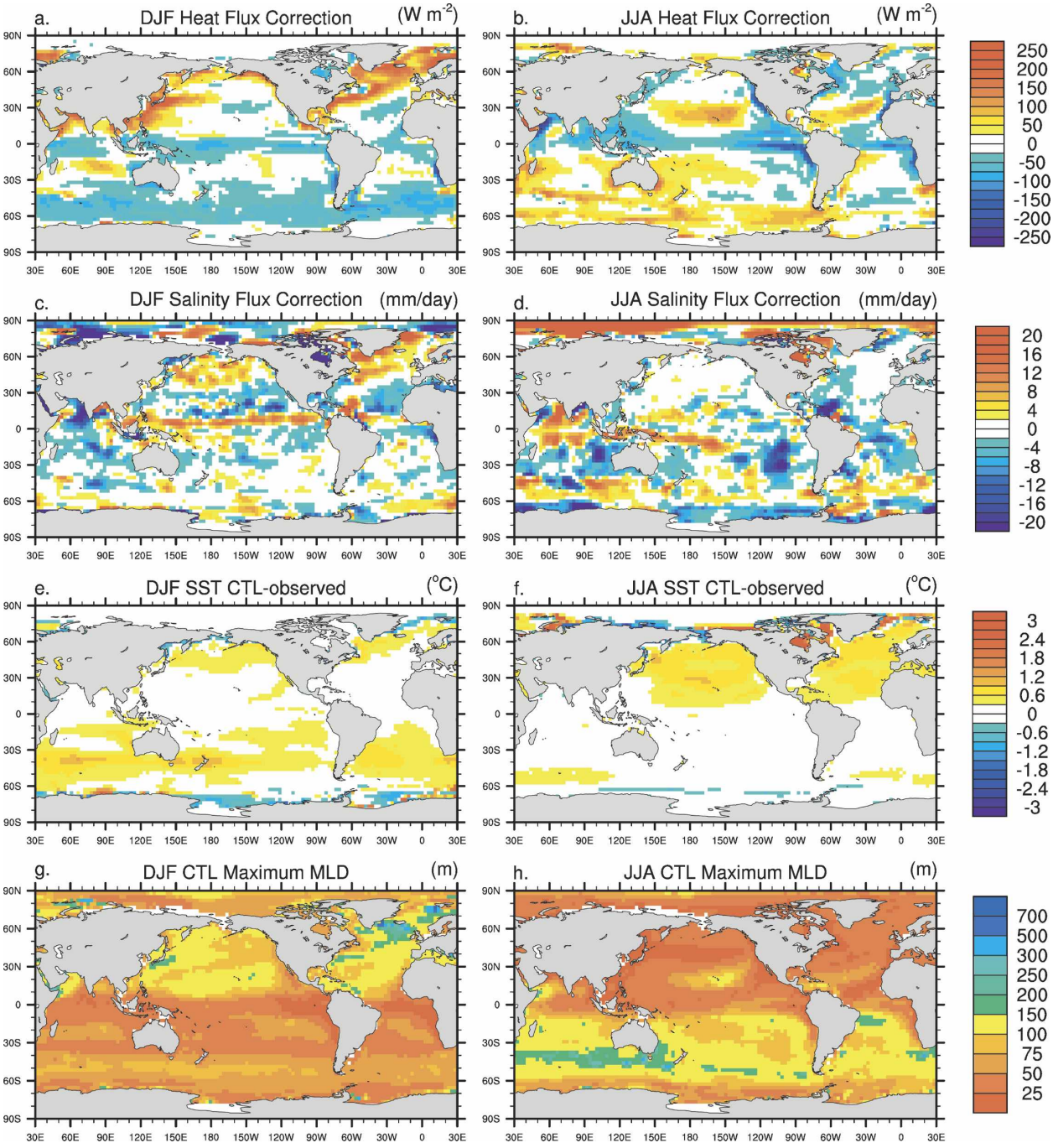

FIG. 1. (a) DJF and (b) JJA average surface heat flux correction (W m^{-2}). Positive values indicate heat is added to the ocean. Shading interval is 25 W m^{-2}. (c) DJF and (d) JJA average surface salinity flux correction (mm day^{-1}). Negative values indicate freshwater is added to the ocean. Shading interval is 2 mm day^{-1}. (e) DJF and (f) JJA average SST bias (°C) given by the difference between the 150-yr mean climatology of CTL SST and the climatology of Hadley Centre Sea Ice and Sea Surface Temperature dataset (HadiSST) SST over 1950–99. Shading interval is 0.3°C. Simulated maximum MLD (m) for (g) boreal and (h) austral winter. Note that the shading interval changes with depth: 25 m for MLD < 100, 50 m for 100 < MLD < 300, and 200 m for deeper MLD.

3. Experimental design

The dominant pattern of reemerging SST anomalies in CTL is identified based on singular value decomposition (SVD; e.g., von Storch and Zwiers 1999) between July and September (JAS; hereafter, 3-month periods are denoted by the first initial of each respective month) subsurface temperature anomalies (40–400-m

TABLE 1. SCF in percentage and correlation coefficient (Corr.) between the SVD PC time series, from lag −8 (NDJ) to 0, with ocean temperature fixed in JAS and SLP lagged as indicated. Boldface denotes significance (95% level confidence) estimated following Czaja and Frankignoul (2002).

Season	NDJ	DJF	JFM	FMA	MAM	AMJ	MJJ	JJA	JAS
SCF	**73**	**79**	**79**	**84**	**64**	**62**	57	53	35
Corr.	0.50	**0.62**	**0.62**	**0.59**	0.45	**0.64**	**0.64**	**0.61**	0.37

depth) in the North Atlantic north of 25°N and SLP anomalies over the North Atlantic–European domain (20°–85°N, 90°W–30°E) at various lead times from the previous November through the concurrent August. In the SVD analysis, the ocean temperature is treated as a vector-valued field and the covariance matrix can be viewed as a collection of submatrices, which contain the covariances between SLP and levels of ocean temperature jointly at the same grid point. Table 1 gives SVD statistics for the leading mode as a function of lead time from November to January (SLP leading ocean temperature by 8 months) to JAS (atmosphere and ocean in phase). The greatest covariances [squared covariance fraction (SCF)] are found between the summer subsurface ocean and the previous winter atmosphere, indicative of the atmosphere forcing the ocean, while contemporaneous or near-contemporaneous ocean–atmosphere covariances are weak and not significant. The heterogeneous spatial patterns of SLP anomalies in February–April and homogeneous subsurface temperature anomalies at 50-m depth in July–September associated with the leading SVD mode that accounts for the largest SCF are shown in Fig. 2. The SLP pattern resembles the NAO, while the subsurface thermal anomaly pattern resembles the North Atlantic tripole. The SLP and subsurface temperature principal component (PC) time series of this SVD mode are dominated by interannual-to-decadal fluctuations and are significantly correlated, as portrayed in Fig. 2c. Our results based on CTL are consistent with the observational findings of Timlin et al. (2002) and de Coëtlogon and Frankignoul (2003). Although the maximum temporal correlation between the PC time series occurs with SLP in May–July, the corresponding pattern of JAS subsur-

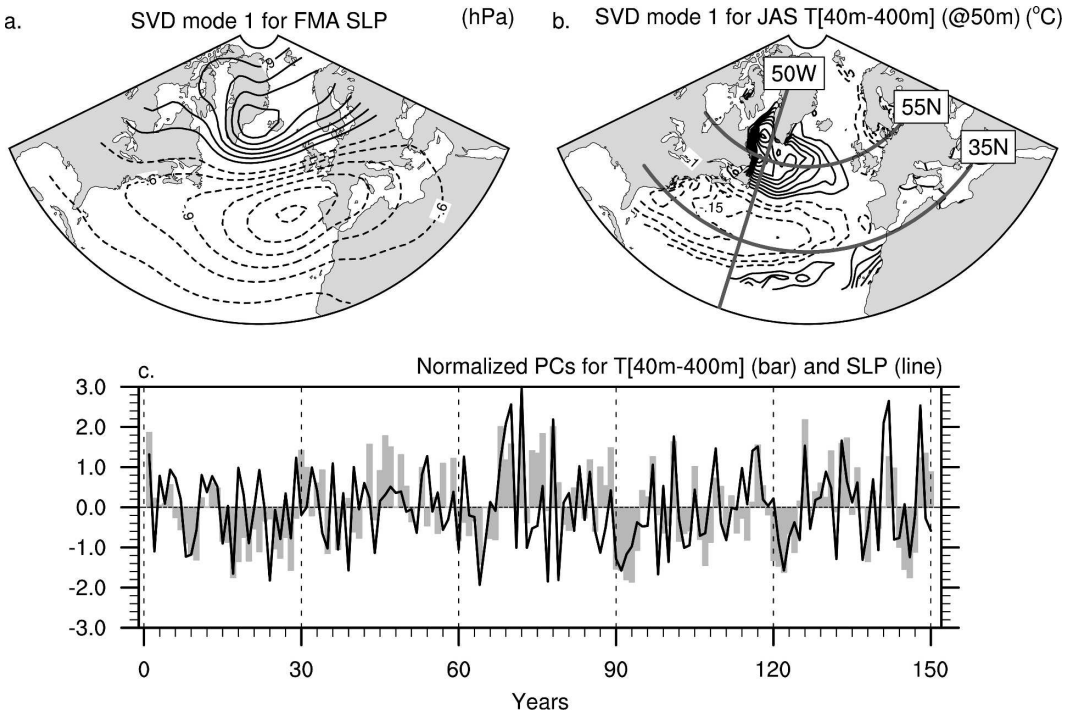

FIG. 2. Leading SVD modes calculated between (a) FMA SLP (hPa) and (b) JAS ocean temperature (T) anomalies (°C) between 40- and 400-m depth, computed from the 150-yr CTL simulation. Contour intervals are 0.3 hPa and 0.05°C, respectively. (c) Corresponding normalized principal component time series of FMA SLP (solid line) and JAS subsurface temperature (bars).

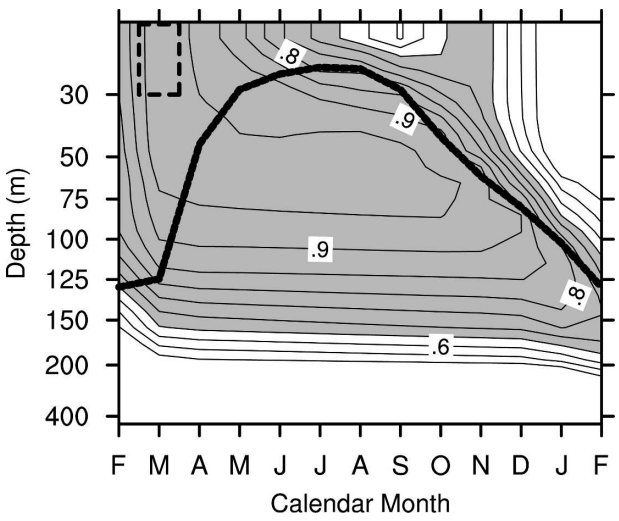

FIG. 3. Simulated CTL lead–lag correlations between the March ocean temperature anomalies averaged over 50°–60°N, 60°–30°W and the first upper 30 m (dashed box), and temperature anomalies between the surface and 450 m, from the previous February through the following February. Contour interval is 0.05 and values in excess of 0.65 are shaded to highlight the reemergence mechanism. The thick superimposed solid line represents the 150-yr climatological mean of the MLD averaged over the domain.

face temperature anomalies is largely confined to the subtropics (25°–30°N) and does not resemble the tripole (not shown). Because our focus is on the extent to which reemergence of the SST tripole pattern influences the atmosphere, we choose the SVD patterns associated with the maximum SCF rather than the maximum PC correlation. In addition, the efficiency of the local and quasi-simultaneous forcing of the atmosphere upon the subsurface ocean in the subtropics is very likely to be overestimated in the model in summer due to exaggerated mixed layer depth south of 30°N (Fig. 1h).

Figure 3 shows the signature of the reemergence mechanism in the northern center of action (50°–60°N, 60°–30°W) of the subsurface temperature SVD pattern, obtained by correlating March temperature anomalies averaged over 0–30-m depth with temperature anomalies as a function of month and depth over the same domain. While correlation values near the surface (0–30 m) decline from April until the following September, those at depth (50–100 m) exhibit almost no attenuation, corroborating the SVD results. A portion of the signal (indicated by correlation values greater than 0.65) rebounds to the surface in October and November in phase with the seasonal deepening of the mixed layer. Thereafter, the correlations decay rapidly along the entire mixed column, similar to observations although less pronounced. Such a decrease is consistent with the effect of entrainment, which mixes the existing heat content anomalies with thermal anomalies newly created by the wintertime atmospheric anomalies. In CTL, the rapid loss of memory is amplified compared to nature as the North Atlantic MLD is underestimated and because the simulated NAO is characterized by a too-strong quasi-biannual component (not shown), thus considerably reducing its winter-to-winter persistence compared to observations. The impact of the reemerging thermal anomalies on the atmosphere is consequently hard to extract from CTL only; however Fig. 3 shows that reemergence indeed occurs in the coupled model.

To isolate and determine the influence of reemergence of the SST tripole upon the atmosphere, two 60-member ensembles of coupled experiments, hereafter REM+ and REM−, are performed based on the FMA atmosphere/JAS ocean SVD results. All members of each ensemble are integrated for a year starting on 1 August with the same perturbed initial oceanic conditions but different initial atmospheric states. The common ocean conditions correspond to the three-dimensional thermal anomalies given by the SVD mode that are added in REM+ (subtracted in REM−) to the 150-yr averaged 1 August ocean conditions computed from CTL. The atmospheric conditions are taken randomly among the one hundred and fifty 1 August atmospheric conditions from CTL. The spatial shape and magnitude of the imposed ocean perturbations are obtained by multiplying the three-dimensional SVD oceanic mode by the maximum value of the SLP PC time series shown in Fig. 2c to preserve linear relations between the variables. The maximum value of the SLP PC time series (3.1) corresponds to an anomalous pressure gradient between the Icelandic Low and Azores High of approximately 12 hPa, similar to observations for a moderate-to-strong NAO (Hurrell et al. 2003). As illustrated in Fig. 4, maximum amplitudes of the REM+ perturbations are found in the western part of the North Atlantic basin and reach 1.2°C in the Labrador Sea (Fig. 4a) and −0.8°C off the east coast of the United States (Fig. 4b). Anomalies are mostly confined between 40- and 125-m depth, below the summer mixed layer of CTL (thick solid curve) but within the winter mixed layer (thick dashed curve). Note that the subsurface temperature anomaly patterns in REM+ and REM− are derived from the coupled model as opposed to observations in order to be consistent with the model physics, thereby maximizing the model sensitivity to the reemergence process. As suggested by numerous studies (see Kushnir et al. 2002 for a review), a spatial match between surface ocean anomalies and atmospheric entities (position of the jet, intensity of the storm track, etc.) appears to be an important factor in

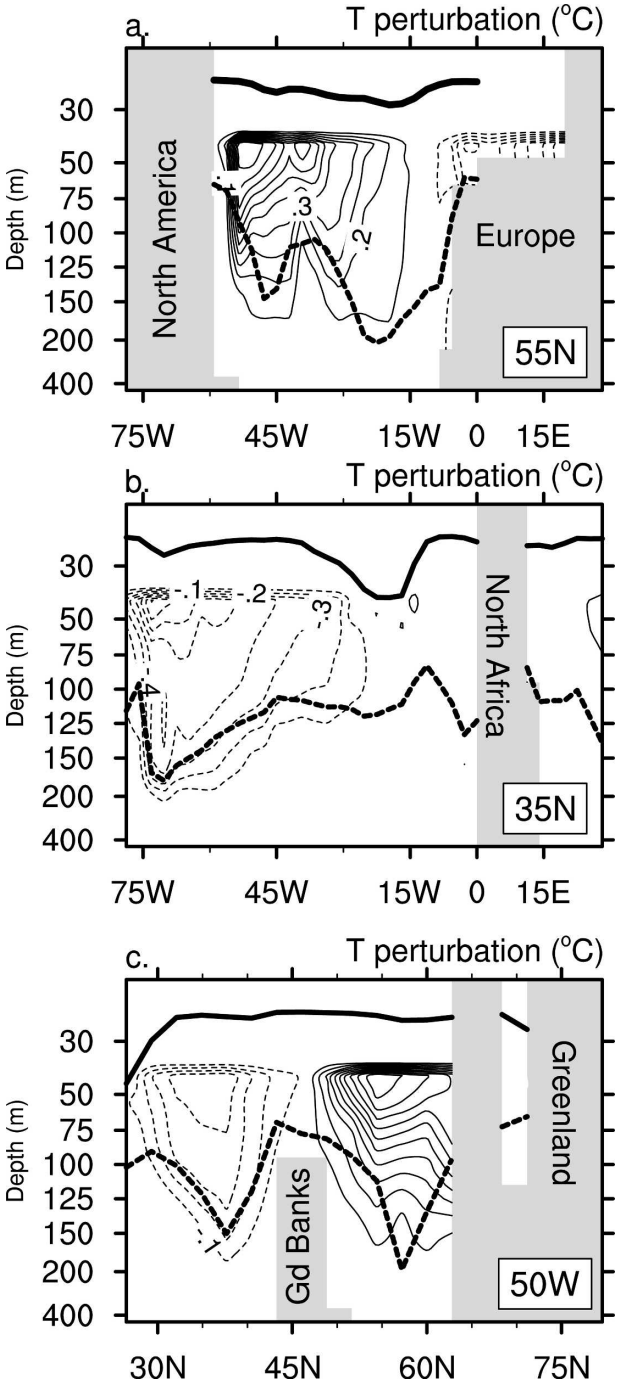

FIG. 4. Anomalous 3D temperature patterns (°C) added to (subtracted from) 1 Aug initial oceanic conditions for REM+ (REM−) and represented here for three ocean sections given in the lower-right corner (drawn in Fig. 2b) as a function of depth. The solid (dashed) thick black line stands for the climatological August (January) MLD simulated in CTL. Contour interval is 0.1°C.

the midlatitude atmospheric response to midlatitude SST anomalies. However, the spatial pattern of the simulated subsurface temperature anomalies is shifted slightly northward compared to observations (de Coëtlogon and Frankignoul 2003) due to the northward displacement of the NAO in the coupled model and the stand-alone atmospheric model (not shown). In the following analysis, we examine mainly the linear portion of the coupled model response by taking the ensemble-mean difference between REM+ and REM−, hereafter referred to as REM.

4. Results

a. Temporal evolution of the simulated ocean anomalies

The monthly evolution of the REM temperature anomalies at 50-m depth (hereafter T50; left panels) and at the surface (right panels) are contrasted in Fig. 5. The midlatitude ocean pattern imposed in the MLM initial conditions is well preserved at the subsurface in September but has yet to appear at the surface. Weak SST signals develop by October and then amplify over the northernmost part of the basin in November and in midlatitudes during in December. The latter mimic the subsurface temperature anomalies, which are, by contrast, concomitantly damped between October and November in the Labrador Sea, and between November and December for regions off the east coast of the United States. From December onward, the surface and subsurface patterns match perfectly, and both intensify slightly in January and then decrease gradually through the following spring.

The temporal evolution of the simulated ocean anomalies is examined further using Fig. 6, which shows the daily values of the vertical entrainment (Q_{we}) contribution and the surface heat flux (Q_{net}) contribution in the mixed layer temperature change (see the above-mentioned Web site for MLM equations). Over the Labrador Sea (LAB.OCE box defined in Fig. 5), the heating rate due to entrainment rapidly increases and significantly contributes to the mixed layer warming from mid-September to mid-November (Fig. 6a). It is particularly active in late October where the temperature anomalies imposed below the seasonal thermocline in the sensitivity experiments are brought back into the deepening mixed layer. Such timing is consistent with the mean seasonal evolution of the MLD presented previously in Fig. 3 for CTL and leads to a significant drop of the temperature anomalies at T50. SST and T50 are identical when MLD exceeds 50 m, that is, around mid-December, while the Q_{we} contribution pro-

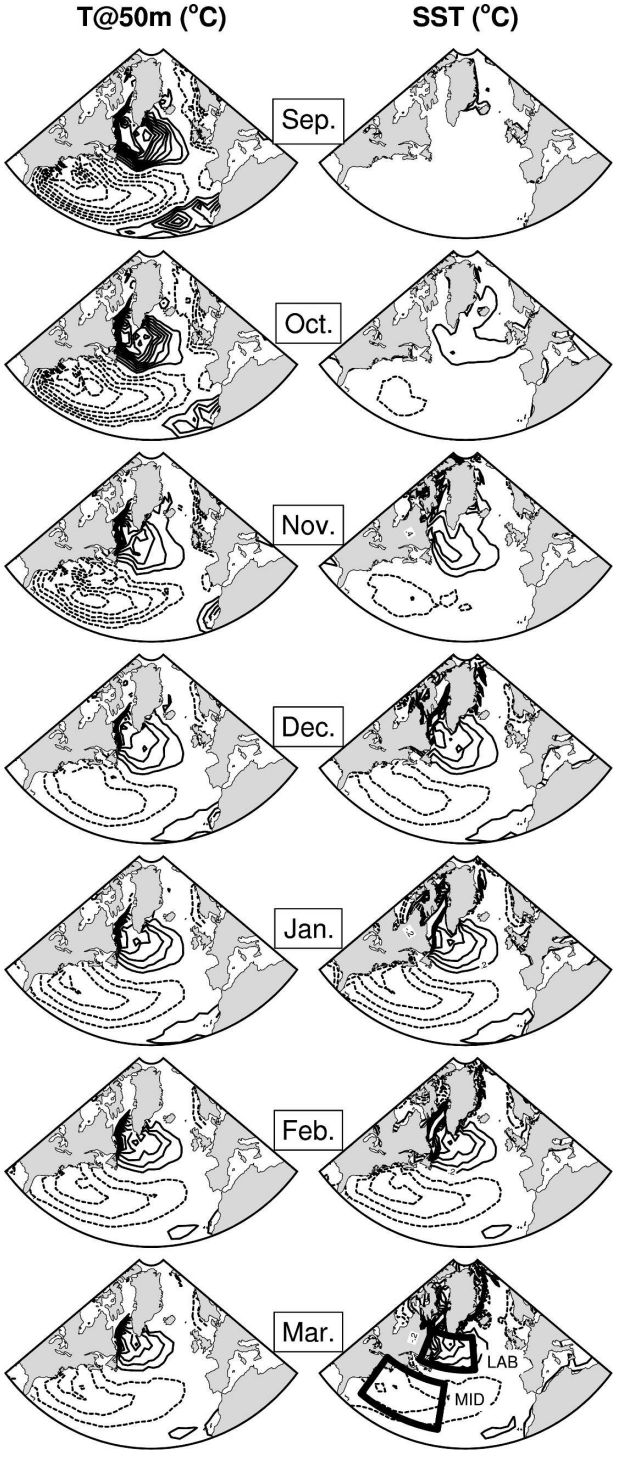

FIG. 5. Temporal evolution of the REM temperature anomalies (°C) at (left) 50-m depth and (right) the surface from September to March. Contour interval is 0.2°C. LAB (50°–60°N, 60°–30°W) and MID (30°–45°N, 75°–45°W) domains used subsequently for oceanic averaged fields are shown on the March SST panel. The entire reemerging SST pattern is statistically significant from November onward (95% significance level based on Student's t statistic) for values greater than ±0.2° (not shown).

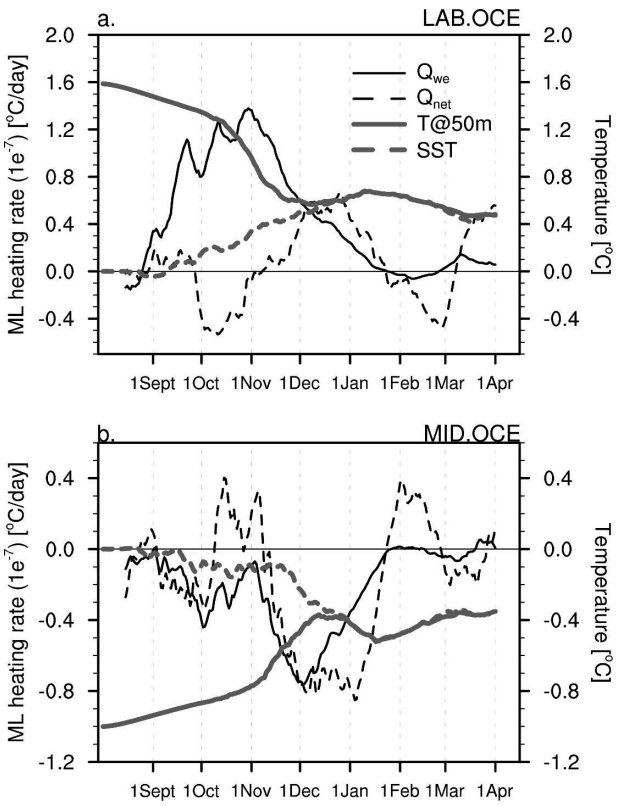

FIG. 6. Temporal evolution (from 1 Aug to 1 Apr) of the simulated REM anomalies averaged over the (a) LAB.OCE and (b) MID.OCE oceanic domains for temperature anomalies at 50-m depth (T50; thick gray) and SST (dashed gray), and for the mixed layer heating rate due to entrainment (Q_{we}; solid thin black line) and due to surface fluxes (Q_{net}; dashed thin black line). A 15-day running mean has been applied to Q quantities, and units are °C and 1×10^{-7} °C day^{-1}, respectively.

gressively diminishes. From January onward, the SST changes are mostly controlled by Q_{net}. Note that Q_{net} tends to counteract the entrainment forcing in early fall, reducing the rate of SST warming, while it amplifies the SST anomalies from December onward, as suggested by Fig. 5. Similar results are found for the mid-Atlantic oceanic region (MID.OCE) with a one-month delay (Fig. 6b). Maximum cooling due to reentrainment at the base of the mixed layer in response to the presence of negative thermal anomalies occurs in late November in phase with the seasonal deepening of the mixed layer for that region (not shown). Negative SST anomalies develop rapidly at the beginning of December, while T50 anomalies are damped. The two anomalies coincide by the end of December, and are further reinforced by the Q_{net} contribution. The evolution of Q_{net} is similar at mid- and high latitudes, whereas all oceanic quantities are delayed by one month in the mid-latitudes relative to the high latitudes. February

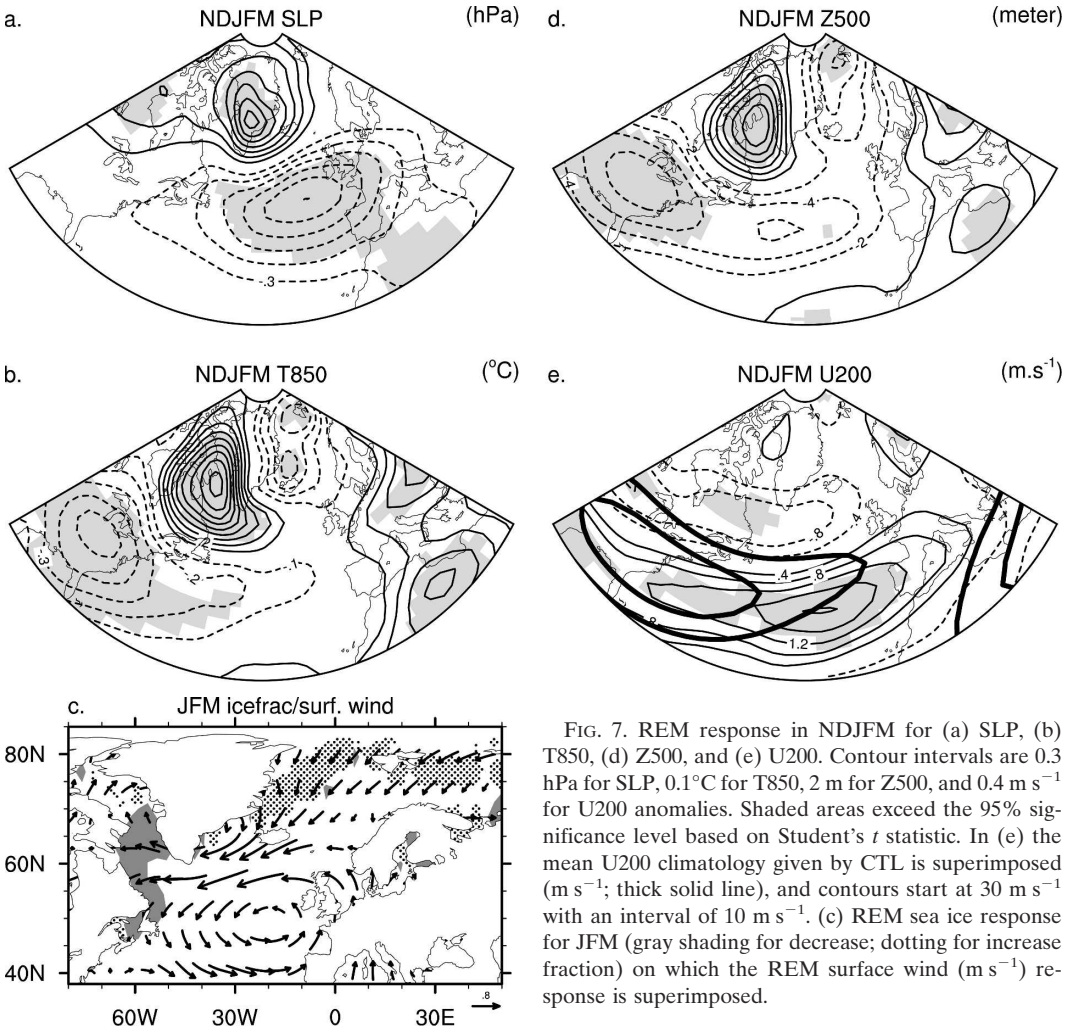

FIG. 7. REM response in NDJFM for (a) SLP, (b) T850, (d) Z500, and (e) U200. Contour intervals are 0.3 hPa for SLP, 0.1°C for T850, 2 m for Z500, and 0.4 m s^{-1} for U200 anomalies. Shaded areas exceed the 95% significance level based on Student's t statistic. In (e) the mean U200 climatology given by CTL is superimposed (m s^{-1}; thick solid line), and contours start at 30 m s^{-1} with an interval of 10 m s^{-1}. (c) REM sea ice response for JFM (gray shading for decrease; dotting for increase fraction) on which the REM surface wind (m s^{-1}) response is superimposed.

differs from the other winter months as Q_{net} damps the SST anomalies in both domains before amplifying them from March onward.

Collectively, the results show that the SST anomalies developing in the REM sensitivity experiments at the beginning of winter are forced by the reemergence process. In particular, we have shown that Q_{we} dominates Q_{net} in their genesis. Thus model experiments can be used to further isolate and investigate the impact of reemergence upon the atmospheric circulation.

b. *Mean atmospheric model response to reemerging SST anomalies*

The ensemble mean REM atmospheric response for November–March is shown in Fig. 7. The simulated SLP pattern exhibits negative values over midlatitudes and positive values over Greenland, with maximum anomalies ~1.8 hPa (Fig. 7a). This response projects strongly on the negative phase of the NAO, the same phase that was used to construct the temperature at depth in summer, and thus represents a positive feedback. Both centers of action are shifted northward compared to the NAO canonical structure estimated from the leading empirical orthogonal function (EOF) of SLP displayed in Fig. 8a for CTL. The REM response is also more confined to the central and western part of the basin and does not include the eastward extension of the Icelandic center toward Scandinavia. As shown in Fig. 8b, the amplitude of the response to reemergence represents 20% (25%) of the interannual standard deviation of winter SLP in CTL locally within the Icelandic (Azores) center of action.

The low-level temperature response at 850 hPa (T850) is westward shifted compared to SLP, with maximum negative (positive) anomalies over North America (Labrador Sea) (Fig. 7b). The positive anomalies over the Labrador Sea and negative anomalies over

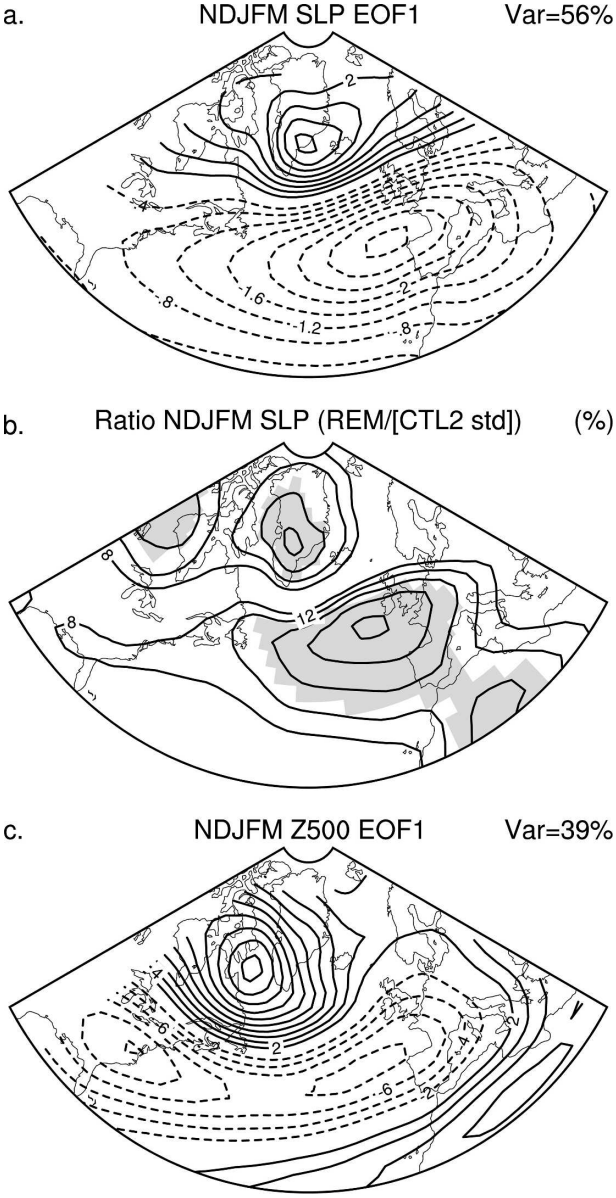

FIG. 8. Leading EOF of (a) NDJFM SLP and (c) Z500 computed from the 150-yr CTL integration. Contour intervals are 0.4 hPa and 2 m, respectively. The variance explained by the EOF is given in the upper-right corner of the pattern (%). (b) Ratio between the NDJFM REM/2 SLP response and the standard deviation of NDJFM SLP computed from CTL. The REM response can be considered as a biased estimated of the reemerging SST-forced signal and the ratio can be interpreted as an averaged measure of the reemergence contribution in the CTL NDJFM interannual variability of SLP. Shading is the same as in Fig. 7a, and contour intervals are 4% starting from 8%.

the Greenland Sea are associated with reduced and increased ice cover, respectively, as shown in Fig. 7c. The changes in ice cover can be related to reduced (enhanced) northwesterly winds over the Labrador (Greenland) Sea associated with the NAO-like large-scale SLP response, similar to observations (Deser et al. 2000). Note that T850 signals are weak over Europe, while they represent about 30%–35% of the total T850 standard deviation estimated from CTL over the eastern United States (not shown).

The upper-level atmospheric REM response is shown in Figs. 7d,e. Geopotential height anomalies at 500 hPa (Z500) strongly resemble the T850 pattern, with amplitudes corresponding to an ~10–20 m $°C^{-1}$ of SST anomaly. The geopotential height response projects onto the upper-level NAO pattern intrinsic to the atmospheric model as estimated in Fig. 8c from the leading Z500 EOF of CTL. The latter is shifted westward compared to the observed NAO (not shown, but see Hurrell et al. 2003). The CAM model tends to overestimate the westward tilt with height of the extratropical modes of variability, and such a bias may contribute to explaining the relatively strong upstream response over the North American continent in T850. The REM Z500 response reflects the T850 anomalies, particularly over the continents and regions of anomalous sea ice [Greenland–Iceland–Norwegian (GIN) Seas]. The 200-hPa zonal wind response (U200) is less affected than T850 and exhibits a zonally elongated north–south dipole corresponding to a reinforcement and eastward extension of the climatological subtropical upper-level jet, in good agreement with the negative NAO phase (Cassou and Terray 2001). The largest wind anomalies are found around 40°N/20°W, on the diffluence side of the jet and are associated with a significant change in storm activity as discussed in the next section.

We have verified that SST anomalies that could potentially contribute to the atmospheric response in REM, especially those in the Tropics, do not develop outside the forcing domain. Similarly, tropical rainfall is not significantly modified in REM, except for a few isolated grid points in the far western tropical Pacific (20°N–20°S, 120°–150°E) that barely pass significance tests. The latter are not associated with any local SST changes and their amplitude is very small (at most 0.12 mm day^{-1}); we thus do not expect them to significantly alter the circulation over the North Atlantic domain.

c. Early winter response and storm-track analysis

Based on model sensitivity experiments, we have shown that oceanic reemergence may contribute to enhancing the year-to-year persistence of the wintertime NAO and SST tripole patterns. What are the physical mechanisms responsible for the recurrence of the NAO from one winter to the next in response to reemergence? Results have been presented so far in terms of the mean winter response during November–March; we

next focus on the timing of the model response within the winter season and the role of midlatitude synoptic eddies in the evolution of the mean atmospheric response.

The evolution of the atmospheric temperature response as a function of height is shown in Fig. 9a over the LAB.ATM domain (52°–62°N, 80°–45°W); note that this region is slightly shifted northwestward compared to its oceanic counterpart (see Fig. 5), as motivated by Fig. 7b. Reemergence warms the low-level atmosphere (below 700 hPa) in October–November, and the warming then rapidly amplifies and extends into the upper troposphere during December. This vertical extension indicates that the atmospheric response is approximately equivalent barotropic from December to February, as confirmed by monthly geopotential height anomaly maps (not shown). Warming then persists at low levels in the following spring consistent with the positive feedback associated with the return of the negative phase of the simulated NAO.

We now focus on the change of the character of the model response between the early stage of reemergence (1 October–15 November, hereafter ES) and the late stage (15 November–31 December, hereafter LS), when vertical export of the atmospheric warming occurs. The precise choice for these two periods is based on the sign of the surface heat flux (Q_{net}) contribution to the mixed layer temperature change (Fig. 6), and on the rapid amplification of the geopotential height response around 15 November at high latitudes (not shown). Damping of the developing SST anomalies occurs basinwide in ES (Fig. 9b) followed by a clear sign reversal (positive SST anomalies collocated with positive heat flux penetrating the surface ocean) in LS, leading to the amplification of the reemerging SST anomalies and the development of the North Atlantic tripole from mid-November onward (Fig. 9c).

The association between the surface fluxes and the dynamics of the atmospheric response is explored separately for the ES and LS periods (Fig. 10). During ES, the SLP response (Fig. 10a) is confined over Europe but is weak and not significant. The surface heat exchange pattern resembles the reemerging anomalies and acts to damp the SST anomalies mainly due to the longwave radiation component that dominates sensible and latent changes.

In contrast to ES, the SLP response in LS is large scale and resembles the negative phase of the NAO. The sign of Q_{net} (which acts to reinforce the SST anomalies) is almost entirely controlled by associated changes in latent and sensible heat fluxes. The rapid and strong development of the large-scale atmospheric response is hypothesized to be linked to atmospheric

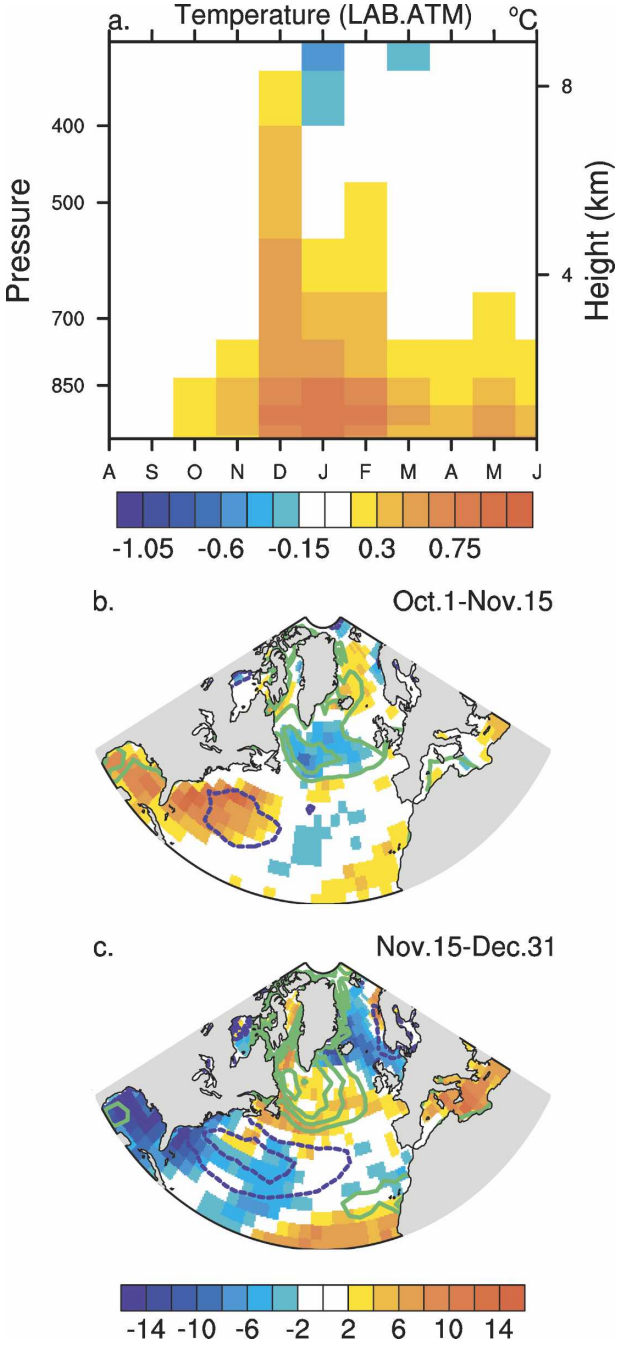

FIG. 9. (a) Temporal evolution as a function of height and pressure of the monthly REM response for temperature (°C) spatially averaged over the LAB.ATM (52°–62°N, 80°–45°W) domain. (b), (c) REM response for total heat flux at the surface (W m^{-2}; color shading) and superimposed REM SST anomalies [°C; green (purple) contour for positive (negative) values; contour interval is every 0.2°C] averaged (b) from 1 Oct to 15 Nov, and (c) from 15 Nov to 31 Dec.

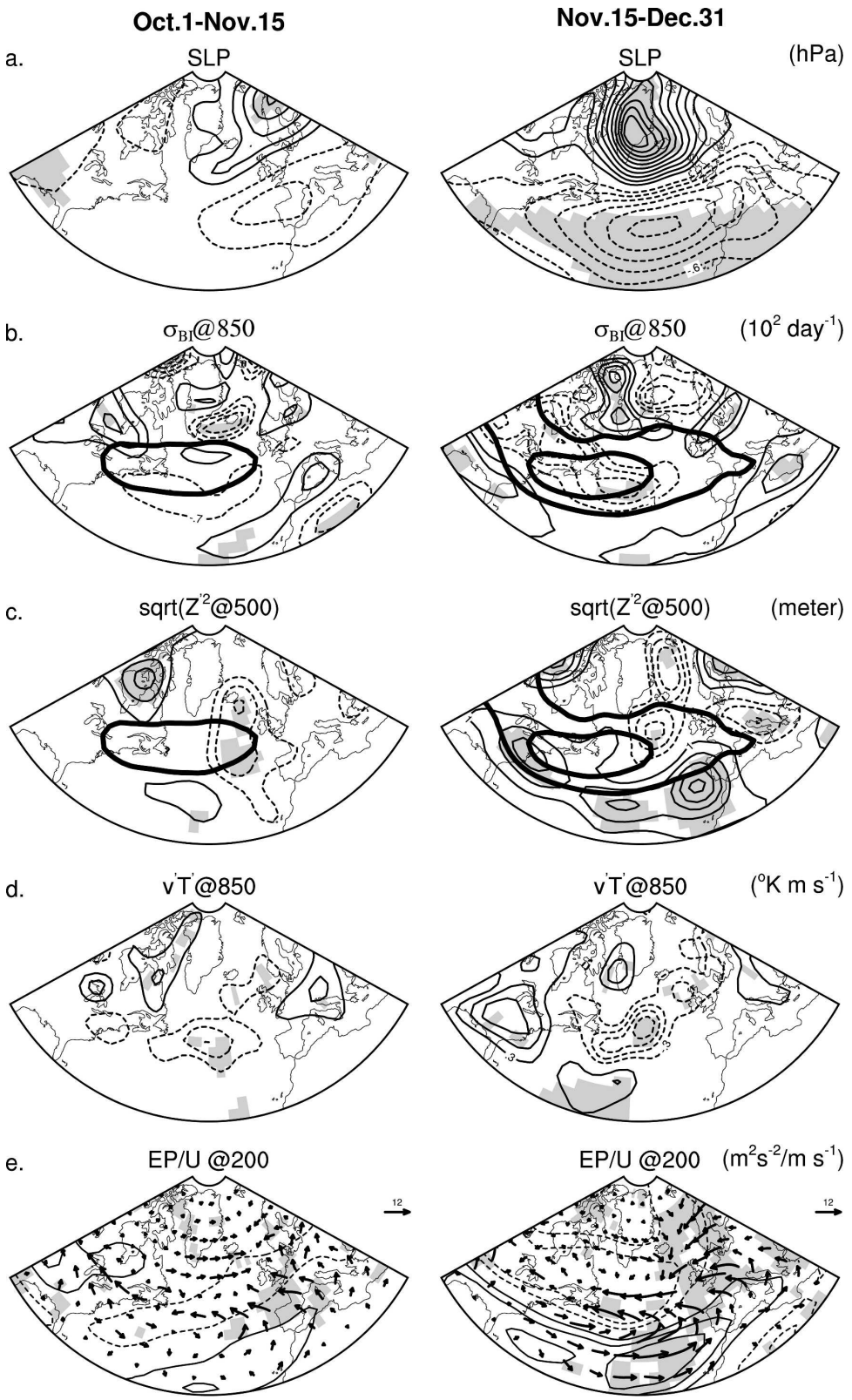
Oct.1-Nov.15
Nov.15-Dec.31
a.
SLP
SLP
(hPa)
b.
σ_{BI}@850
σ_{BI}@850
(10^2 day^{-1})
c.
sqrt(Z'^{2}@500)
sqrt(Z'^{2}@500)
(meter)
d.
v'T'@850
v'T'@850
(°K m s^{-1})
e.
EP/U @200
EP/U @200
(m^{2}s^{-2}/m s^{-1})
12
12

transient eddy activity. The low-level baroclinicity (Fig. 10b), estimated from the Eady baroclinic instability growth rate maximum parameter σ_{BI} (Hoskins and Valdes 1990), exhibits a decrease due to a reduced SST gradient at the intergyre boundary off Newfoundland. The anomalous SST gradient is local and weak in ES while it is large scale and significant in LS, coinciding with the position of the storm track and its seasonal development. A clear and significant southward shift of the storm track is found in LS as shown by the anomalous variance of the bandpass (2.2–6 day) filtered Z500 (Fig. 10c). Storminess is significantly enhanced (diminished) at midlatitudes (high latitudes) over and downstream of the cold (warm) reemerging SST anomalies (recall Fig. 5). The associated large-scale strengthening (slackening) of the westerlies is consistent with the change in sign of the atmospheric feedback effect (see Frankignoul 1985 and Kushnir et al. 2002 for reviews) on the SST anomalies between ES and LS (Fig. 9). The storm-track alterations also lead to a reduction in the anomalous poleward heat flux by the transient eddies (hereafter v′T′850; Fig. 10d), consistent with the presence of anomalously warm conditions in the Labrador Sea that reduce the climatological gradient between the two oceanic gyres. Note that, although clearly amplified in LS, the anomalous v′T′850 can also be found in ES but is substantially weaker and does not seem to affect the upper-level atmosphere via transient eddy dynamics.

Perturbations in the transient eddy momentum fluxes computed from Eliassen–Palm (EP) vector diagnostics (Trenberth 1986) are shown in Fig. 10e. The divergence (convergence) of EP is indicative of mean flow acceleration (deceleration) due to the presence of storm-track activity changes. During ES, EP fluxes are locally confined to the eastern side of the Atlantic basin and are barely significant. For LS, a clear divergence occurs in the model on the southeastern side of the subtropical climatological jet (~35°N, 40°–10°W) and is compensated to the north by a strong convergence in the jet exit region off the British Isles and along the eddy-driven jet off Newfoundland. Such an anomaly is consistent with enhanced zonality of the basic flow (Doblas-Reyes et al. 2001) as shown in Fig. 10e by the superimposed U200 anomalies, and with the forcing tendency due to synoptic eddies to develop a large-scale negative NAO pattern.

d. Role of internal variability and nonlinearity

As noted in the introduction, there is an emerging consensus that the internal variability in an atmospheric general circulation model plays a strong role in shaping the pattern of the forced response (Peng and Robinson 2001; Magnusdottir et al. 2004; Deser et al. 2004). To examine this aspect and to gain insight into the nonlinearity of the response, we decompose the REM November–March mean atmospheric response into daily circulation patterns or weather regimes, which are internal structures of variability: a modification of the climate mean state can be interpreted as the integration of the changes in their intrinsic frequency of occurrence. We identify the dominant weather regimes using cluster analysis (the *k*-means algorithm: Michelangeli et al. 1995) applied to raw daily (instantaneous values at 0000 UTC) SLP anomalies from REM+, REM−, and 60 yr (randomly selected) from the 150-yr control integration of the model for a total of 27 180 daily SLP anomaly maps (3 ensembles × 60 members × 151 days per extended winter). The significance of the results is tested following Farrara et al. (2000), and the method used to compute the regimes is described in greater detail by Cassou et al. (2004). The regimes estimated from Z500 are very similar to those obtained from SLP (not shown).

Four weather regimes have been extracted, corresponding to the optimal partition based on the so-called classificability index detailed in Michelangeli et al. (1995) and applied to our dataset (Fig. 11). We verified that these regimes are the same as those obtained using only data from the entire 150-yr control integration or from stand-alone integrations of the atmospheric model forced with a repeating seasonal cycle of SST and sea ice conditions. The first regime, termed GE for Greenland–Europe, projects on the positive phase of the NAO, although compared to observations the two centers of action are northward shifted and the anomalously deep subpolar low is located over Greenland instead of Iceland. The second regime, termed IL+, is

←

FIG. 10. REM response averaged (left) from 1 Oct to 15 Nov, and (right) from 15 Nov to 31 Dec for (a) SLP, (b) Eady growth rate of baroclinic instabilities σ_{BI}, (c) storm-track activity estimated by $(Z'^2)^{1/2}$ computed from 2.2–6-day bandpass-filtered Z500, (d) meridional heat transport by the storms estimated by $v'T'$ computed at 850 hPa (v′T′850) from 2.2–6-day bandpass filter quantities, and (e) zonal wind at 200 hPa (U200) on which anomalous Eliassen–Palm vectors are superimposed. Contour intervals are 0.3 hPa for SLP, 0.7×10^{-2} day^{-1} for σ_{BI}, 1 m for storm track activity, 0.3 K m s^{-1} for $v'T'$, and 0.4 m s^{-1} for U200 anomalies. Shaded areas exceed the 95% significance level based on the Student's *t* statistic. The mean storm-track climatology given by CTL is superimposed on the anomalous σ_{BI} and storm-track maps (m; thick solid line) and contours start at 50 m with a contour interval of 15 m.

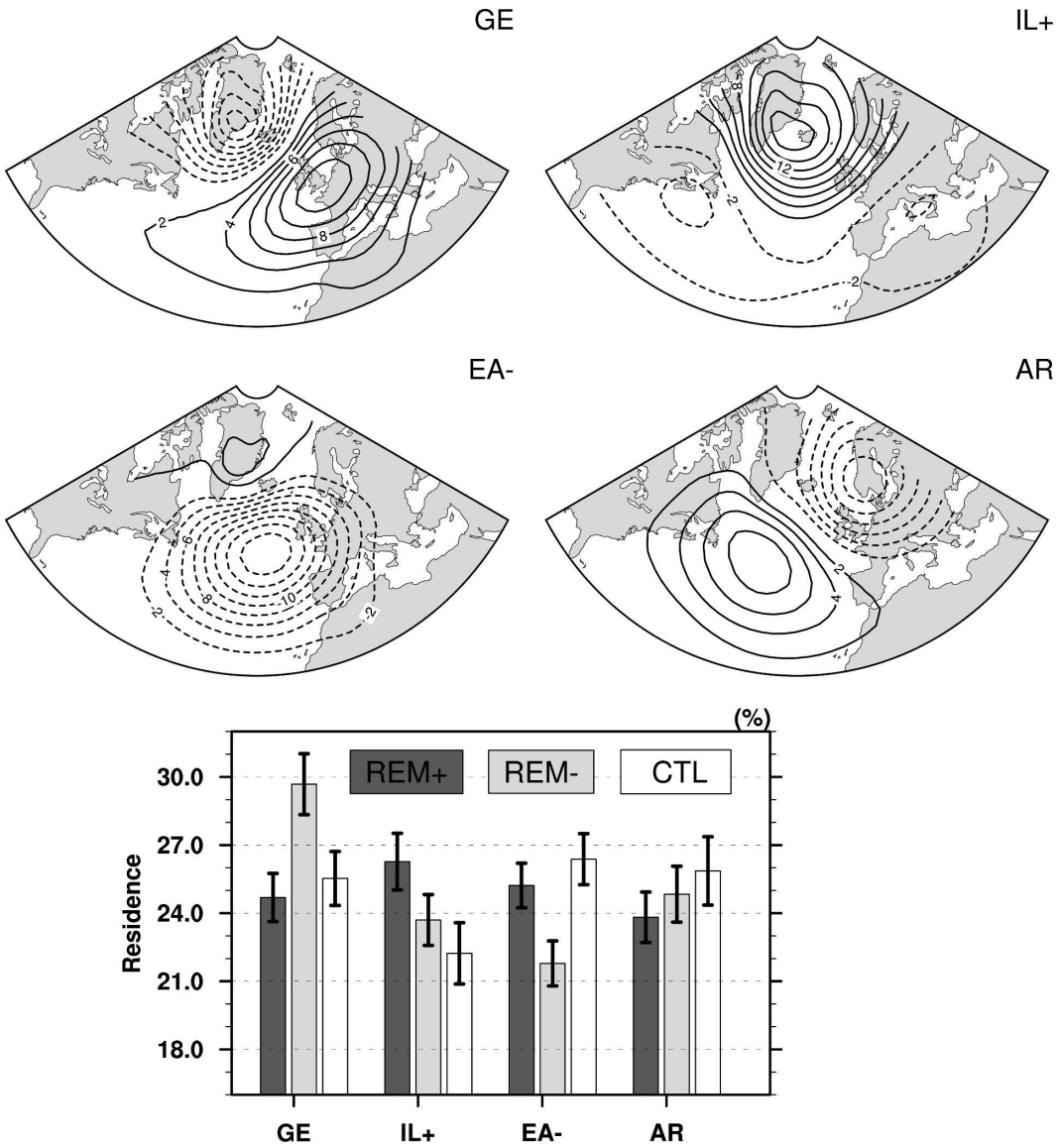

FIG. 11. (top) Leading four weather regimes (GE, EA−, IL+, and AR) based on daily SLP anomaly maps from the from REM+, REM−, and CTL experiments. Contour interval is 2 hPa. (bottom) Histograms showing the percent daily occurrences of the four weather regimes for REM+, REM−, and CTL experiments. The error bars correspond to the maximum dispersion of the decomposition when the clustering is performed on anomaly maps with respect to individual experiment means (Farrara et al. 2000).

characterized by a strong and dominant positive SLP anomaly centered over Iceland, with weaker-amplitude negative anomalies in midlatitudes; this pattern projects somewhat onto the negative phase of the NAO. The third regime exhibits low pressure that extends over most of the basin and is reminiscent of the negative phase of the east Atlantic mode (Barnston and Livezey 1987) and is thus termed EA−. The fourth regime strongly projects onto the Atlantic Ridge (AR) pattern despite a clear northwestward displacement of the positive core toward Canada compared to observations (Cassou et al. 2004).

The frequencies of occurrence for the four regimes in REM+, REM−, and CTL are shown in the bottom panel of Fig. 11. Comparing REM+ and REM− reveals that the reemergence mostly affects the excitation of the GE and EA− regimes, while IL+ and AR occurrences are not significantly altered. The GE regime is favored by about 6% in REM− compared to REM+, that is, when cold (warm) subsurface anomalies re-

emerge in the Labrador Sea (at midlatitudes). EA− occurs more (less) often when the Labrador Sea is warm (cold) and the midlatitude ocean is cold (warm). These results help in the interpretation of the mean SLP response (Fig. 7a) that can now be understood as the average of changes in the excitation of two internal regimes. In other words, the ocean forcing does not fix the phase or amplitude of a mode of variability but rather slightly changes the occurrence of regimes. This explains why the mean forced response does not strictly project onto the canonical NAO as discussed previously, but reflects a combination of the GE and the EA patterns of internal variability

As a final step, the nonlinearity of the model response as a function of the sign of the reemerging SST tripole may be assessed by comparing the frequencies of occurrence for REM+ compared to CTL and REM− compared to CTL. REM+ differs from CTL in terms of IL+, whereas REM− differs from CTL in both GE and EA−. The REM+ response is consistent with Peng and Robinson (2001), showing the presence of an equivalent barotropic ridge immediately downstream of positive SST anomalies located in the subpolar gyre (Fig. 2b). The nature of the REM− response can be understood following the same mechanism. Warm midlatitude SST anomalies along 35°N (opposite to Fig. 2b) favor the GE regime that is characterized by raising of geopotential height surfaces above and downstream of these anomalies. At the same time, the ocean anomalies diminish the excitation of the EA− regime dominated by a trough located downstream of the anomalies, and projecting on the opposite phase of GE. The fact that different regimes are altered between REM+ and REM− is expected to be controlled by how strongly the SST-forced direct response projects on the regimes themselves, which are mostly controlled by internal eddy-driven dynamics. It is beyond the scope of this paper to examine in further detail the nonlinearity of the model response.

5. Summary and discussion

A coupled model consisting of an atmospheric GCM, an entraining ocean mixed layer model, and a thermodynamic sea ice model has been developed to examine the impact of winter-to-winter reemergence of SST anomalies in the North Atlantic upon the atmospheric circulation. The reemergence mechanism is first evaluated in the model through a long 150-yr control integration from which we extract via SVD analysis the dominant structure of oceanic thermal variability below the summer mixed layer that is related to the previous late-winter atmospheric forcing. This pattern closely resembles the North Atlantic SST tripole created by the previous wintertime NAO. The associated three-dimensional thermal anomalies are then imposed in the ocean initial conditions of two 60-member ensemble experiments (one with positive polarity and one with negative polarity) of coupled simulations of 1-yr duration starting in August. These thermal anomalies are included only between 40 and 400 m (below the summer mixed layer) and north of 25°N, thus keeping the surface ocean unperturbed in line with the reemergence paradigm. We verify that the imposed thermal anomalies are reentrained into the seasonally deepening mixed layer at the beginning of winter, and generate significant SST anomalies at that time.

Exposed to the reemerging oceanic thermal perturbation, the model atmosphere develops a mean quasi-barotropic response that strongly projects onto the NAO. The sign of the NAO response is the same as that which generated the oceanic thermal anomalies in the previous winter, thus contributing to winter-to-winter persistence of the NAO. The amplitude of the response is 10–20 m at 500 hPa per °C, representing locally about 20%–25% of the interannual standard deviation estimated from the control simulation. The amplitude of the reemergence-induced signal is thus comparable to any other externally forced signals (cf. Kushnir et al. 2002).

Transient eddies along the North Atlantic storm track play a significant role in shaping the structure of the large-scale atmospheric response, as well as in controlling its timing. Classical diagnostics indicate that the transient eddies have a positive feedback on the mean flow from mid-November onward. The low-level atmospheric anomalies along the storm track are present at the early stage of reemergence (October), whereas upper-level fields are not altered except locally over Europe (Fig. 10). This suggests that the perturbation in the meridional SST gradient may not be exported to upper levels before mid-November because the mean circulation is not sufficiently dynamically active (the SST gradient is not significantly enhanced in mid-November, arguing against a direct SST-gradient mechanism). This further highlights the importance of the mean seasonal flow, in particular the position and strength of the upper-level jet with respect to the SST anomalies as suggested by Peng and Robinson (2001). The delayed atmospheric response may also be due to the time scale for atmospheric adjustment to midlatitude SST anomalies as discussed in Ferreira and Frankignoul (2005) and Deser et al. (2007).

The mean winter atmospheric response may also be interpreted in terms of weather regime. We showed that the linear portion of the reemergence mechanism

alters the occurrence of the positive GE regime (which projects strongly onto the positive phase of the NAO) and negative EA regime. The regime paradigm may help to explain why the response to extratropical SST anomalies is model dependent, that is, the difference in model sensitivity may result from the spatial coherence between the direct SST-forced signal and the spatial properties of the regimes controlled by internal dynamics, leading to a more or less pronounced reorganization of their occurrence.

Despite the fact that we chose to apply realistic amplitude subsurface thermal perturbations leading to realistic amplitude reemerging SST anomalies, the magnitude of the atmospheric response is detectable and comparable to that due to other sources ($\sim$10–20 m K^{-1} at 500 hPa) as reviewed in Kushnir et al. (2002). It would be of great interest to reproduce similar sensitivity experiments with other coupled models to better assess the robustness of the spatial pattern and magnitude of the atmospheric response to reemerging North Atlantic SST anomalies. The model response obtained here might be artificially enhanced due to biases in the CAM2 mean state: for example, the modes of variability and in particular their signatures at middle and upper levels are considerably westward shifted in CAM2 compared to observations and are collocated with the regions where the imposed ocean thermal anomalies are the strongest. On the other hand, the sensitivity of the coupled model could be considered as too conservative due to the shallower-than-observed simulated wintertime MLD, which reduces the amount of energy stored in the entire mixed oceanic column.

The results of this study do not preclude the impact of oceanic processes such as advection, diffusion, eddy mixing, and subduction upon the persistence of the mixed layer temperature anomalies and the NAO. Advection could shift the reemergence pattern and subduction could weaken it as discussed in de Coëtlogon and Frankignoul (2003). The impact of advection/mixing on reemergence has been examined in the Pacific in Sugimoto and Hanawa (2005), and more studies would be needed for the Atlantic. In addition, the investigation of effects of thermal anomalies onto the atmosphere was restricted to those connected to the SST tripole forced by the NAO. Even if the latter is the most persistent and the NAO is the most effective forcing, it is conceivable that other reemerging anomalies may influence the extratropical atmosphere. Further quantitative assessment of the effects of dynamical ocean processes versus mixed layer physics (such as the reemergence mechanism) is needed for a more complete understanding of interannual and longer time-scale SST variability in midlatitudes.

Acknowledgments. We thank J. W. Hurrell and L. Terray for very stimulating discussions. We are also very grateful to A. S. Phillips for his technical assistance. The figures were produced with the NCL software developed at NCAR, and the simulations were carried out using the NCAR-SCD facilities under the CSL project. This work was supported in part by NOAA under Grant NA06GP0394 and by CNRS and by the European Community via the sixth framework ENSEMBLES project under Contract GOCE-CT-2003-505539.

REFERENCES

Alexander, M. A., and C. Deser, 1995: A mechanism for the recurrence of wintertime midlatitude SST anomalies. *J. Phys. Oceanogr.,* **25,** 122–137.

——, ——, and M. S. Timlin, 1999: The reemergence of SST anomalies in the North Pacific Ocean. *J. Climate,* **12,** 2419–2433.

——, J. D. Scott, and C. Deser, 2000: Processes that influence sea surface temperature and ocean mixed layer depth variability in a coupled model. *J. Geophys. Res.,* **105,** 16 823–16 842.

Barnston, A. G., and R. E. Livezey, 1987: Classification, seasonality and persistence of low-frequency atmospheric circulation patterns. *Mon. Wea. Rev.,* **115,** 1083–1126.

Briegleb, B. P., C. M. Blitz, E. C. Hunke, W. H. Lipscomb, M. M. Holland, J. L. Schramm, and R. E. Moritz, 2004: Scientific description of the sea ice component in the Community Climate System Model, Version 3. NCAR Tech. Note NCAR/TN463+STR, 70 pp.

Cassou, C., and L. Terray, 2001: Dual influence of Atlantic and Pacific SST anomalies on the North Atlantic/Europe winter climate. *Geophys. Res. Lett.,* **28,** 3195–3198.

——, ——, J. W. Hurrell, and C. Deser, 2004: North Atlantic winter climate regimes: Spatial asymmetry, stationarity with time, and oceanic forcing. *J. Climate,* **17,** 1055–1068.

Cayan, D. R., 1992: Latent and sensible heat flux anomalies over the northern oceans: Driving the sea surface temperature. *J. Phys. Oceanogr.,* **22,** 859–881.

Czaja, A., and C. Frankignoul, 2002: Observed impact of Atlantic SST anomalies on the North Atlantic Oscillation. *J. Climate,* **15,** 606–623.

de Boyer Montégut, C. E., G. Madec, A. S. Fischer, A. Lazar, and D. Iudicone, 2004: Mixed layer depth over the global ocean: An examination of profile data and a profile-based climatology. *J. Geophys. Res.,* **109,** C12003, doi:10.1029/2004JC002378.

de Coëtlogon, G., and C. Frankignoul, 2003: On the persistence of winter sea surface temperature in the North Atlantic. *J. Climate,* **16,** 1364–1377.

Deser, C., and M. S. Timlin, 1997: Atmosphere–ocean interaction on weekly timescales in the North Atlantic and Pacific. *J. Climate,* **10,** 393–408.

——, J. E. Walsh, and M. S. Timlin, 2000: Arctic sea ice variability in the context of recent atmospheric circulation trends. *J. Climate,* **13,** 617–633.

——, M. A. Alexander, and M. S. Timlin, 2003: Understanding the persistence of sea surface temperature anomalies in midlatitudes. *J. Climate,* **16,** 57–72.

——, G. Magnusdottir, R. Saravanan, and A. Phillips, 2004: The effects of North Atlantic SST and sea ice anomalies on the winter circulation in CCM3. Part II: Direct and indirect components of the response. *J. Climate,* **17,** 877–889.

——, R. A. Tomas, and S. Peng, 2007: The transient atmospheric circulation response to North Atlantic SST and sea ice anomalies. *J. Climate,* in press.

Doblas-Reyes, F. J., M. A. Pastor, J. M. Casado, and M. Déqué, 2001: Wintertime westward traveling planetary scale perturbations over the Euro-Atlantic region. *Climate Dyn.,* **17,** 811–824.

Farrara, J. D., C. R. Mechoso, and A. W. Robertson, 2000: Ensembles of AGCM two-tier predictions and simulations of the circulation anomalies during winter 1997–1998. *Mon. Wea. Rev.,* **128,** 3589–3604.

Feldstein, S. B., 2000: The timescale, power spectra, and climate noise properties of teleconnection patterns. *J. Climate,* **13,** 4430–4440.

Ferreira, D., and C. Frankignoul, 2005: The transient atmospheric response to midlatitude SST anomalies. *J. Climate,* **18,** 1049–1067.

Frankignoul, C., 1985: Sea surface temperature anomalies, planetary waves and air–sea feedback in middle latitudes. *Rev. Geophys.,* **23,** 357–390.

Gaspar, P., 1988: Modeling the seasonal cycle of the upper ocean. *J. Phys. Oceanogr.,* **18,** 161–180.

Greatbatch, R. T., 2000: The North Atlantic Oscillation. *Stochastic Environ. Res. Risk Assess.,* **14,** 213–242.

Hoskins, B. J., and P. J. Valdes, 1990: On the existence of storm-tracks. *J. Atmos. Sci.,* **47,** 1854–1864.

Hurrell, J. W., 1995: Decadal trends in the North Atlantic oscillation: Regional temperatures and precipitation. *Science,* **269,** 676–679.

——, Y. Kushnir, G. Ottersen, and M. Visbeck, 2003: An overview of the North Atlantic Oscillation. *North Atlantic Oscillation: Climate Significance and Environmental Impact, Geophys. Monogr.,* Vol. 134, Amer. Geophys. Union, 1–22.

Junge, M. M., and T. W. N. Haine, 2001: Mechanisms of North Atlantic wintertime sea surface temperature anomalies. *J. Climate,* **14,** 4560–4572.

Kiehl, J. T., and P. R. Gent, 2004: The Community Climate System Model, version 2. *J. Climate,* **17,** 3666–3682.

Kushnir, Y., W. A. Robinson, I. Bladé, N. M. J. Hall, S. Peng, and R. Sutton, 2002: Atmospheric GCM response to extratropical SST anomalies: Synthesis and evaluation. *J. Climate,* **15,** 2233–2256.

Madden, R. A., 1976: Estimates of the natural variability of time-averaged sea-level pressure. *Mon. Wea. Rev.,* **104,** 942–952.

Magnusdottir, G., C. Deser, and R. Saravanan, 2004: The effects of North Atlantic SST and sea ice anomalies on the winter circulation in CCM3. Part I: Main features and storm track characteristics of the response. *J. Climate,* **17,** 857–876.

Michelangeli, P.-A., R. Vautard, and B. Legras, 1995: Weather regimes: Recurrence and quasi stationarity. *J. Atmos. Sci.,* **52,** 1237–1256.

Oleson, K. W., and Coauthors, 2004: Technical description of the Community Land Model (CLM). NCAR Tech. Note NCAR/TN-461+STR, 174 pp.

Peng, S., and W. A. Robinson, 2001: Relationships between atmospheric internal variability and the responses to an extratropical SST anomaly. *J. Climate,* **14,** 2943–2959.

Rodwell, M. J., 2003: On the predictability of North Atlantic climate. *North Atlantic Oscillation: Climate Significance and Environmental Impact, Geophys. Monogr.,* Vol. 134, Amer. Geophys. Union, 173–192.

Seager, R., Y. Kushnir, M. Visbeck, N. Naik, J. Miller, G. Krahmann, and H. Cullen, 2000: Causes of Atlantic Ocean climate variability between 1958 and 1998. *J. Climate,* **13,** 2845–2862.

Stephenson, D. B., V. Pavan, and R. Bojariu, 2000: Is the North Atlantic a random walk? *Int. J. Climatol.,* **20,** 1–18.

Sugimoto, S., and K. Hanawa, 2005: Remote reemergence areas of winter sea surface temperature anomalies in the North Pacific. *Geophys. Res. Lett.,* **32,** L01606, doi:10.1029/2004GL021410.

Timlin, M. S., M. A. Alexander, and C. Deser, 2002: On the reemergence of North Atlantic SST anomalies. *J. Climate,* **15,** 2707–2712.

Trenberth, K. E., 1986: An assessment of the impact of transient eddies on the zonal flow during a blocking episode using localized Eliassen–Palm flux diagnostics. *J. Atmos. Sci.,* **43,** 2070–2087.

von Storch, H., and F. W. Zwiers, 1999: *Statistical Analysis in Climate Research.* Cambridge University Press, 484 pp.

Watanabe, M., and M. Kimoto, 2000: On the persistence of decadal SST anomalies in the North Atlantic. *J. Climate,* **13,** 3017–3028.

Wunsch, C., 1999: The interpretation of short climate records, with comments on the North Atlantic and Southern Oscillations. *Bull. Amer. Meteor. Soc.,* **80,** 245–255.